Applied Catalysis B: Environmental 168-169 (2015) 441–447

Contents lists available at ScienceDirect

Applied Catalysis B: Environmental

journal homepage: www.elsevier.com/locate/apcatb

E. coli inactivation by visible light irradiation using a Fe–Cd/TiO_2 photocatalyst: Statistical analysis and optimization of operating parameters

Mehrzad Feilizadeh[a,b], Guido Mul[a,*], Manouchehr Vossoughi[b,c]

[a] *Photocatalytic Synthesis Group, Faculty of Science and Technology, MESA+ Institute for Nanotechnology, University of Twente, P.O. Box 217, 7500 AE Enschede, The Netherlands*
[b] *Department of Chemical and Petroleum Engineering, Sharif University of Technology, Tehran, Iran*
[c] *Institute for Biotechnology and Environment, Sharif University of Technology, Tehran, Iran*

ARTICLE INFO

Article history:
Received 6 October 2014
Received in revised form
17 December 2014
Accepted 21 December 2014
Available online 16 January 2015

Keywords:
Fe–Cd-doped TiO_2
Visible light
Disinfection
Operating parameters
Response surface methodology

ABSTRACT

In this study, the antibacterial effect of a Fe and Cd co-doped TiO_2 (Fe–Cd/TiO_2) visible light sensitive photocatalyst was optimized by varying operating parameters and using a response surface methodology to evaluate the experimental data. Twenty sets of disinfection experiments were conducted by adjusting three operating parameters, *i.e.* initial pH of the solution, reaction temperature and catalyst loading, at five levels. Based on the experimental data, a semi-empirical model was established and subsequently applied to predict the final concentration of *Escherichia coli* after 45 min exposure to the catalyst and visible light irradiation. Using the accurate model (coefficient of determination $R^2 = 0.963$), optimum values were found to be 40.1 °C, 6.3, and 1.0 g/L for reaction temperature, initial pH of solution and photocatalyst loading, respectively. Under the optimized conditions, the Fe–Cd/TiO_2 catalyst achieved a bacterial inactivation efficiency of 99.9% after 45 min of visible light illumination.

1. Introduction

Over the last few years, the availability of clean water has significantly decreased, and purification by removal of chemical and microbiological contaminations is necessary before use [1,2]. Conventional methods of water purification and disinfection such as chlorination, germicidal UV-C exposure, and ozonation are often chemically, energetically or operationally expensive, which often prevents practical implementation [2–4]. Alternatively, advanced oxidation processes (AOPs) based on light activated TiO_2 have attracted much attention, which rely on the *in situ* formation of highly reactive chemical species capable of destroying biological water contaminants [4–7]. However, practical application of TiO_2 is constrained due to its unfavorable optical properties [8,9]. In particular, it is of great interest to modify TiO_2 in order to enhance its photocatalytic response to visible light irradiation [10].

Many attempts have been made to shift the onset of TiO_2 absorption from the ultraviolet to the visible region, while maintaining a large reactive surface [11,12]. One of the most effective methods is doping of TiO_2 with different metal ions, such as Fe^{3+} and Cd^{2+} [13–18]. Fe^{3+}-doping introduces new states in the bandgap of TiO_2, and thus, increases the efficiency of absorption of visible light [15]. It has been reported that the presence of Cd^{2+} typically decreases the tendency of crystal growth of TiO_2, and thus results in a large reactive surface area and consequently higher photocatalytic efficiency [16,17]. It should be noted that none of the above mentioned studies on Fe^{3+} and Cd^{2+} doping in TiO_2 have reported leaching of Fe^{3+} and Cd^{2+}, potentially being an issue for practical application.

In the present work, we combined the mentioned properties of Fe^{3+} and Cd^{2+} doping in TiO_2, to establish efficient water disinfection under visible light irradiation. We have conducted an extensive evaluation of the effect of operating parameters on *Escherischia coli* inactivation efficiency, *i.e.,* reaction temperature, solution pH and catalyst loading, which are reported among the most important in water disinfection processes [19–29]. Most of the research up to now applied a 'one-variable-at-a-time' (OVAT) approach. OVAT overlooks simultaneous interactions of variables; therefore, it can be unreliable for the optimization of process variables [30]. A Response surface methodology (RSM) based on statistical design of experiments (DOEs), yields more reliable correlations, and was applied in the present study on the basis of a minimum number of experiments [31,32]. Using the obtained contour and surface

* Corresponding author. Tel.: +31 53 4893890; fax: +31 53 4892882.
E-mail address: g.mul@utwente.nl (G. Mul).

http://dx.doi.org/10.1016/j.apcatb.2014.12.034
0926-3373/

response plots, the optimized operational conditions for a high *E. coli* inactivation efficiency were determined. To the best of the author's knowledge, no publication to date has demonstrated the use of RSM to optimize operating parameters of photocatalytic water disinfection under visible light irradiation.

2. Materials and methods

2.1. Catalyst preparation

All chemicals used in this study were reagent-grade and utilized as received without purification. Fe–Cd/TiO_2 (2% Cd, 3% Fe molar ratio) was synthesized using a sol–gel method. The specific molar ratios of the dopants were selected in accordance with optimized activity as reported in our and previous studies [33–37]. In this method, 2.5 mL titanium isopropoxide (TTIP, ≥98%, Sigma–Aldrich) was added into 4.3 mL glacial acetic acid (Merck KgaA, Darmstadt, Germany), and the mixture was stirred vigorously in an ice bath (0 °C) for 30 min, during which time a sol was formed. Then, 53.1 mL deionized water containing stoichiometric amounts of $Fe(NO_3)_3.9H_2O$ (Merck KgaA, Darmstadt, Germany) and $Cd(NO_3)_2.4H_2O$ (Merck KgaA, Darmstadt, Germany), was added dropwise. The prepared mixture was sonicated at 0 °C for 20 min and subsequently stirred for 2 h. Afterwards, the mixture was kept for a day at room temperature in a dark area. Then, it was gelated at 76 °C for 12 h and dried at 120 °C for 3 h. The dried gel was ground with a mortar and pestle into fine powder and calcined at 550 °C (10 K/min. heating rate) for 3 h. Un-promoted TiO_2 was synthesized similarly to the above method, without addition of the Fe^{3+} and Cd^{2+} precursor salts.

2.2. Characterization of synthesized photocatalysts

The X-ray diffraction (XRD) patterns of the synthesized nanophotocatalysts were recorded using a Philips (X'pert Pro MPD) X-ray diffractometer with Ni-filtered Cu Kα radiation over the range of 2θ angles from 10° to 80°. The morphology and size of the nanoparticles were analyzed by scanning electron microscope (SEM, Philips S360 MV2300) and transmission electron microscopy (TEM; Phillips CM10). Moreover, energy dispersive X-ray (EDX) spectra were also obtained by scanning electron microscopy (Philips S360 MV2300). Diffuse reflectance spectra (DRS) of the catalysts were recorded using an Avaspec-2048-TEC spectrophotometer. The point of zero charge (PZC) of the Fe–Cd/TiO_2 was calculated by measuring the zeta potential, ζ of the sample at different pH values using a ZetaPlus zeta-potential analyzer (Brookhaven Instruments Corporation).

2.3. E. coli inactivation experiments

The inactivation experiments were carried out using a Pyrex glass beaker of 250 ml (7 cm in diameter and 9 cm in height) as a batch reactor. The reaction mixture was stirred and illuminated for 45 min. Four 50 W tungsten-halogen lamps (Spark Light, G5.3, 220 V) with a 400-nm cutoff filter (Kenko Co.) were used as the visible light source providing a light intensity of 46.3 mW/cm^2 at the entry point of the reactor. The lamps were fixed 10 cm in distance from the surface of the mixture. During the reaction process, air was continuously bubbled so that the concentration of dissolved oxygen was not changed. The photoreactor was placed in an incubator which could provide the desired temperature of the reaction. For each experiment, operating parameters (reaction temperature, catalyst concentration and initial pH of the reaction mixture) were adjusted based on the design of experiment. After optimizing the parameters, two control experiments were conducted under the predicted optimum condition. Control experiments consisted of performing reaction in the absence of catalyst particles, or in the absence of the irradiation source. Moreover, two experiments were conducted using un-promoted TiO_2 and TiO_2 P-25 (Evonik). In addition, for the purpose of evaluation of the reutilization potential and the possibility of leaching of Fe^{3+} or Cd^{2+}, re-suspension of the catalyst in fresh *E. coli* solution was followed by evaluation of the performance according to the steps indicate above. Catalysts were used up to as much as four times.

Table 1
Experimental ranges and levels of the independent variables.

Variables	Ranges and levels				
	$-\alpha$	−1	0	+1	$+\alpha$
Reaction temperature (A, °C)	25.00	30.07	37.50	44.93	50
Initial pH of solution (B)	4.00	5.01	6.50	7.99	9.00
Catalyst loading (C, g/L)	0.10	0.28	0.55	0.82	1.00

2.4. Bacterial strain and growth media

E. coli ATCC 11105 was used as a bacterial strain obtained from the bacterial bank of the biotechnology department of the Sharif University of Technology. Before each run, *E. coli* was inoculated into nutrient broth No. 2 (Merck, KgaA, Darmstadt, Germany), and grown overnight at 37 °C by constant agitation under aerobic conditions. From a stationary growth phase, aliquots of the bacterial culture were harvested by centrifugation and the pellets were washed with tryptone solution (Merck, KgaA, Darmstadt, Germany). Then, the bacterial pellets were re-suspended in tryptone solution. In all the photocatalytic inactivation experiments, an initial *E. coli* concentration of 10^7 CFU/mL was used. For the samples taken after each run, analysis of *E. coli* inactivation was performed by serial dilutions and a viable colony method on agar media using the pour plate technique. The number of colonies was counted after incubating at 37 °C for 24 h.

2.5. Experimental design and statistical analysis

The three selected operating parameters; reaction temperature (A, °C), initial pH of solution (B) and catalyst loading (C, g/L) were optimized using RSM. These parameters were considered as independent variables and the concentration of *E. coli* (CFU/mL) after 45 min irradiation was chosen as the response (dependent variable). Central composite design (CCD), which is one of the most usual methods of RSM, was employed to evaluate the effects of the three independent variables on the response using twenty sets of experiments. The levels of independent variables were coded as; $-\alpha$, −1, 0, +1 and $+\alpha$, as illustrated in Table 1. By applying CCD, the obtained experimental results were fitted to an empirical quadratic polynomial model expressed as follows:

$$Y = \beta_0 + \beta_1 A + \beta_2 B + \beta_3 C + \beta_{12} AB + \beta_{13} AC + \beta_{23} BC + \beta_{11} A^2 + \beta_{22} B^2 + \beta_{33} C^2 \quad (1)$$

where, Y is the predicted response, β_0 is the interception coefficient, β_1, β_2 and β_3 are coefficients of the independent variables, β_{11}, β_{22} and β_{23} are quadratic terms and β_{12}, β_{13} and β_{23} are interaction coefficients. Analysis of variance (ANOVA) and an optimization procedure with the assistance of RSM were carried out using Design-Expert® software (Trial version 9.0.3 Stat-Ease, Inc. Minneapolis, USA).

3. Results and discussion

3.1. Characterization of synthesized photocatalyst

Fig. S1, Supporting information, represents the XRD patterns of Fe–Cd/TiO_2 and the synthesized un-promoted ('bare') TiO_2 nanoparticles. There are no rutile peaks (JCPDS 89-4202) present in the patterns of Fe–Cd/TiO_2 and un-promoted TiO_2. Furthermore, X-ray diffraction peaks of both samples were fully indexed with JCPDS XRD file 89-4921, indicating the existence of crystallites of the anatase crystal structure, without the presence of any impurity phase [37,38]. No significant diffraction peaks corresponded to any phase based on Fe species [39,40]. Moreover, $CdTiO_3$ phases were not identified, in agreement with the Ti:Cd molar ratio which is ≤0.5:0.5 in the prepared sample [16,37]. Comparing the peak height and broadness of the anatase phase in the diffractogram of Fe–Cd/TiO_2 and un-promoted TiO_2, respectively, indicates that the mean crystallite size of un-promoted TiO_2 is larger than of Fe–Cd/TiO_2. The Scherrer equation was used to determine the approximate mean crystallite size of the samples:

$$\mathrm{dp} = \frac{0.89\lambda}{\beta\cos\theta} \quad (2)$$

where dp is the mean crystallite size, λ is the wavelength of X-ray radiation (Cu Kα = 1.54 Å), β is the line width at half-maximum height, after subtraction of equipment broadening, and θ is the diffraction angle. The mean crystal size (dp) of Fe–Cd/TiO_2 and the synthesized TiO_2 are 18 nm and 28 nm, respectively. The lower crystal size of the Cd-promoted samples is in agreement with a study of Mohammadi and Fray [16], who propose this to be the result of a decrease in the tendency of TiO_2 for temperature induced crystal growth when Cd-ions are present.

Fig. S2, Supporting information, shows a SEM image of the Fe–Cd/TiO_2 particles. It can be clearly seen that this photocatalyst is composed of spherical nanoparticles with a homogeneous size distribution. Moreover, TEM images (Fig. S3, Supporting information) show that the particles have an average particle size of about 19 nm, in agreement with the XRD analysis.

EDX analysis of the Fe–Cd/TiO_2 catalyst is presented in Fig. S4, Supporting information, confirming the presence of Cd and Fe in the nanophotocatalyst formulation. The distribution percentages of Cd and Fe in the nanoparticles were about 2% and 3%, respectively.

Fig. S5, Supporting information, exhibits the diffuse reflectance spectra of Fe–Cd/TiO_2, and the synthesized un-promoted TiO_2. Results show that doping of TiO_2 with Cd and Fe increases light absorbance in the visible region (between 380 and 760 nm). Therefore, Fe–Cd/TiO_2 is expected to induce greater photocatalytic activity than un-promoted TiO_2 when exposed to visible light [41].

3.2. Statistical analysis

Following the experimental design presented in Table 2, an empirical second order polynomial equation was developed for the response variable (*E. coli* concentration) as a function of the three independent variables as shown in Eq. (3).

$$Y = +110675.4 - 2310.2A - 7705.3B - 72883.3C + 32.8AB + 546.8AC - 2042.8BC + 21.3A^2 + 653.1B^2 + 35217.9C^2 \quad (3)$$

where Y represents the final *E. coli* concentration (CFU/mL) and A, B and C are the reaction temperature (°C), initial pH of solution and catalyst loading (g/L), respectively.

The experimental data for *E. coli* inactivation were statistically investigated by analysis of variance and the results are shown in Table 3. The ANOVA of the second order quadratic polynomial model shows that the model is highly significant, as the *F*-value for the model is 28.7 and the corresponding *P*-value is <0.0001. This means that there is only a 0.01% chance of occurrence of the model *F*-value as a result of noise. The lack of fit of the *F*-value of 4.19 is not significant, as the corresponding *P*-value is >0.05. For a model to be successfully used for prediction, this lack of fit should be insignificant [42,43].

The predicted coefficient of determination value (R^2) of 0.963 is in good agreement with the corresponding adjusted R^2 value of 0.930. The high value of R^2 indicates that the quadratic polynomial equations can be used to predict the *E. coli* inactivation in the experimental range [44]. The predicted values of the final *E. coli* concentration were plotted versus the corresponding observed values in Fig. 1. Moreover, the normal probability plot of the residuals is illustrated in Fig. 2, and it shows that there is almost no violation of the assumptions: errors are normally distributed and independent, while the error variance is homogeneous [45].

Table 2
Central composite design of experiment along with actual and predicted values of the response.

Run	Variables			Final concentration of *E. coli* (CFU/mL)	
	Reaction temperature (°C)	Initial pH of solution	Catalyst loading (g/L)	Actual	Predicted
1	37.5	4	0.55	18200	15926.8
2	50	6.5	0.55	17300	14942.3
3	37.5	6.5	0.55	15100	14073.6
4	44.93	5.01	0.82	10000	10762.2
5	44.93	5.01	0.28	18500	21365.8
6	37.5	6.5	0.55	14800	14073.6
7	37.5	6.5	0.55	12600	14073.6
8	37.5	6.5	1	9400	9093.25
9	37.5	6.5	0.55	15200	14073.6
10	25	6.5	0.55	19500	19868.1
11	30.07	5.01	0.28	27000	27194.7
12	37.5	6.5	0.55	13400	14073.6
13	44.93	7.99	0.28	26300	26365.8
14	30.07	7.99	0.82	14000	12541.1
15	37.5	9	0.55	20200	20383.6
16	30.07	5.01	0.82	11100	12241.1
17	37.5	6.5	0.55	12900	14073.6
18	44.93	7.99	0.82	11300	12512.2
19	30.07	7.99	0.28	30100	30744.7
20	37.5	6.5	0.1	35000	33317.1

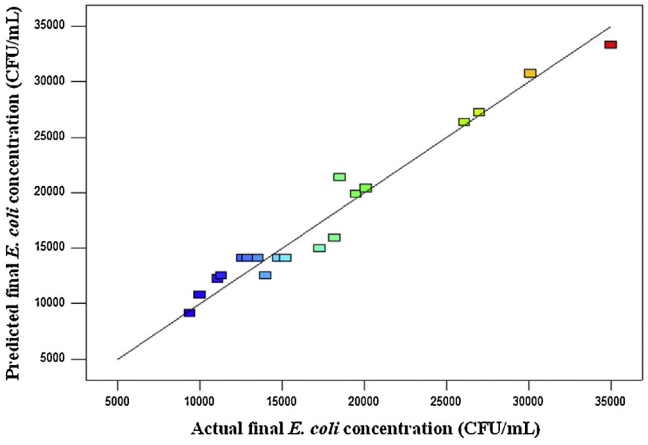

Fig. 1. Plot of the actual and predicted values for the final concentration of *E. coli*.

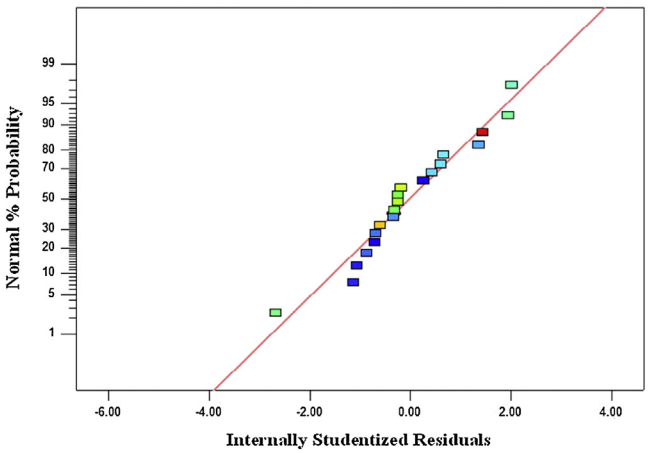

Fig. 2. Plot of the normal probability and internally studentized residuals for the final concentration of *E. coli*.

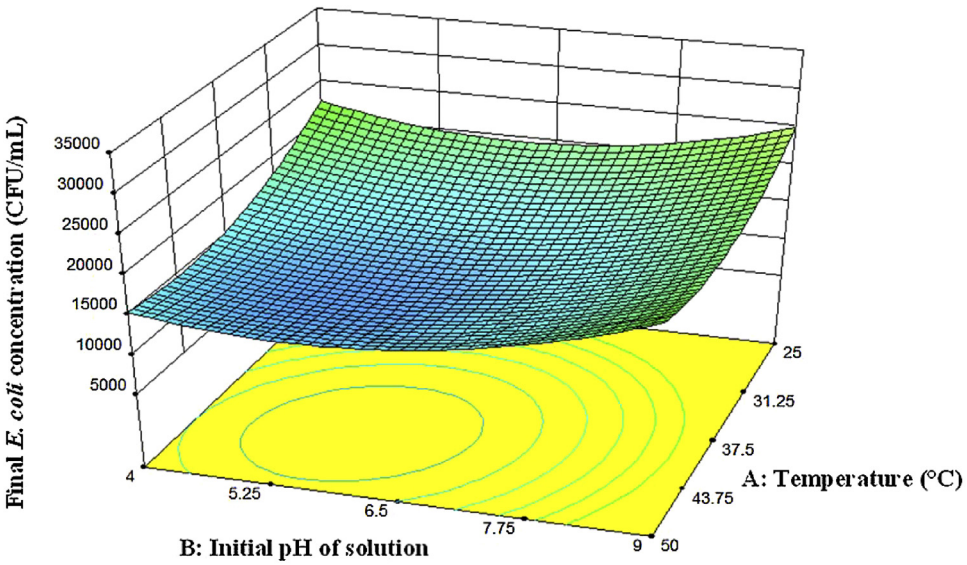

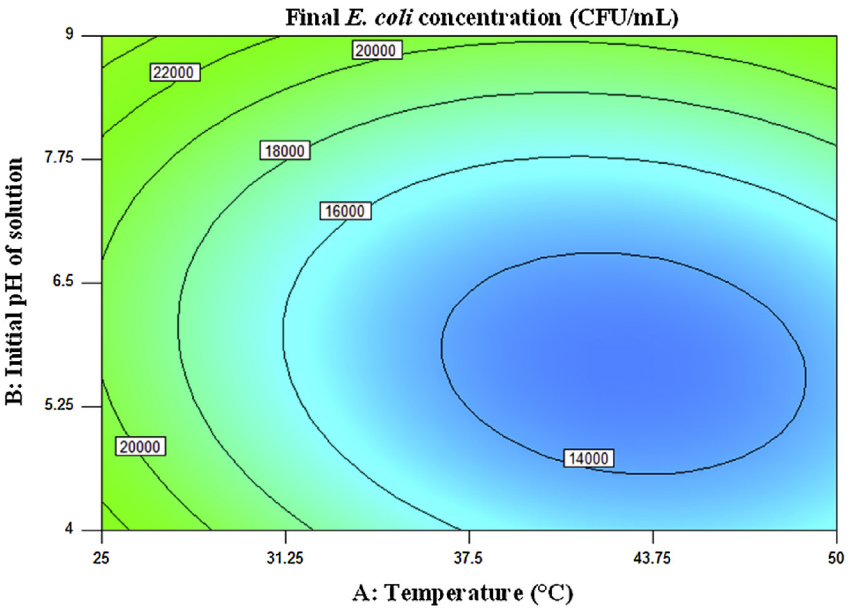

Fig. 3. The response surface plots (a) and contour (b) of the final concentration of *E. coli* as a function of reaction temperature (A) and initial pH of solution (B).

Table 3
ANOVA for the proposed quadratic model.

Source	Sum of squares (SS)	*F*-value	*P*-value
Model	8.99*E*+08	28.71	<0.0001
A	2.93*E*+07	8.41	0.0158
B	2.39*E*+07	6.89	0.0254
C	7.08*E*+08	203.46	<0.0001
AB	1.05*E*+06	0.3	0.4842
AC	9.46*E*+06	2.72	0.1303
BC	5.28*E*+06	1.52	0.2463
A^2	2.00*E*+06	5.74	0.0375
B^2	3.00*E*+07	8.62	0.0149
C^2	9.16*E*+07	26.32	0.0004
Residual	3.48*E*+07	–	–
Lack of fit	2.81*E*+07	4.19	0.0710
Pure error	6.71*E*+06	–	–

R-squared = 0.963; Adj *R*-squared = 0.929; Pred *R*-squared = 0.754.
A: reaction temperature (°C); B: initial pH of solution; C: catalyst loading (C, g/L).

Furthermore, the significance of the coefficients of variables was determined by the *F*-value and the *P*-value. In general, the smaller the *P*-value and the larger the *F*-value, the greater the contribution of the corresponding model term toward the response variable [45]. Therefore, according to Table 3, the catalyst loading was the most influential parameter among the three operating parameters.

3.3. Analysis of contour and response surface plots

After performing all the experiments which were suggested by CCD, the response surface analysis was carried out, in order to investigate of effects of the variables and find optimal conditions for *E. coli* disinfection. Response surface analysis helps in identification of the type of interactions between the selected variables. In Figs. 3–5, response surface plots and the corresponding contour plots of *E. coli* concentration are displayed for the three pairs of the factors.

According to the Fig. 5a and b, the most suitable conditions were moderate temperature (around 40 °C) and a pH of approximately 6. The figures show that both very acidic pH and higher temperature (over 40 °C) conditions lessened *E. coli* inactivation efficiency. In the case of pH, the proper explanation can be that very acidic pH conditions cause the synthesis of acid shock proteins (ASPs) which can result in lower inactivation of *E. coli* [4]. In this regard, Heyde and Portalier [46] reported that after shifting the extracellular pH of *E. coli* from 6.9 to 4.3, seven ASPs were specifically induced for protection against acid-shock. Therefore, the same phenomenon can explain the decreasing inactivation efficiency in the pH range from 5.5 to 2. While, raising the pH from basic to slightly acidic (from 9 to around 6) increased inactivation efficiency of *E. coli* (Figs. 3 and 5). This can be explained by the PZC of the photocatalyst. The measured PZC of the Fe–Cd/TiO_2 photocatalyst was 5.9, which is quite close to the PZC of the pure anatase phase reported in the literature *i.e.*, 6.3 [47,48]. Photocatalyst particles at pH lower than the PZC are charged positively and can induce electrostatic interactions with the bacteria (such as *E. coli*), being negatively charged at these pH values. Hence, a lower pH favors inactivation of *E. coli* [47–51].

In the case of temperature, the main reason of lower disinfection efficiency at high temperatures (40–50 °C) can be attributed to the enhanced recombination rate of the charge carriers, *i.e.*, photo-generated electron–hole pairs. In addition, the adsorption of bacteria onto the photocatalyst surface (which is a spontaneous exothermic phenomenon) decreases at higher temperatures [3,48]. Moreover, synthesis of heat shock proteins, which protect cells against heat and oxidation stresses, can be another reason why the disinfection efficiency decreased at temperatures above 40 °C [52,53]. On the other hand, raising temperature from 25 to 40 °C had a significant positive effect on *E. coli* inactivation. This positive effect of heating on the photocatalytic disinfection of coliforms such as *E. coli* has been previously also reported by Rincon and Pulgarin [20]. They found that the reaction time necessary to achieve complete *E. coli* inactivation was reduced to about one-third by increasing the temperature from 23 to 45 °C.

According to Figs. 4 and 5, *E. coli* inactivation efficiency steadily improved with the increase of the catalyst loading from 0.1 to 1.0 g/L. The main reason is that the number of active sites in the solution increased with catalyst loading [54]. Furthermore, as it can be concluded from these figures, *E. coli* inactivation efficiency is extremely more sensitive to changes in catalyst loading compared with other parameters. This is in agreement with the *P*-values obtained for each parameter from ANOVA.

3.4. Optimization of independent variables and verification of results

The optimal values of the selected variables were obtained using numerical optimization method provided by the Design-Expert 9.0.3 software. The goal of the optimization was to minimize the final concentration of *E. coli* in the solution after irradiation for 45 min. The point at which the final concentration of *E. coli* was predicted to be in its lowest value was found to be 40.1 °C, 6.3, and 1.0 g/L for reaction temperature, initial pH of the solution and catalyst loading, respectively. Based on the suggested model (Eq. (2)), final concentration of *E. coli* under the optimal condition should be 9260 CFU/mL.

To confirm the accuracy of the optimization, duplicate verification experiments were carried out. The average final concentration

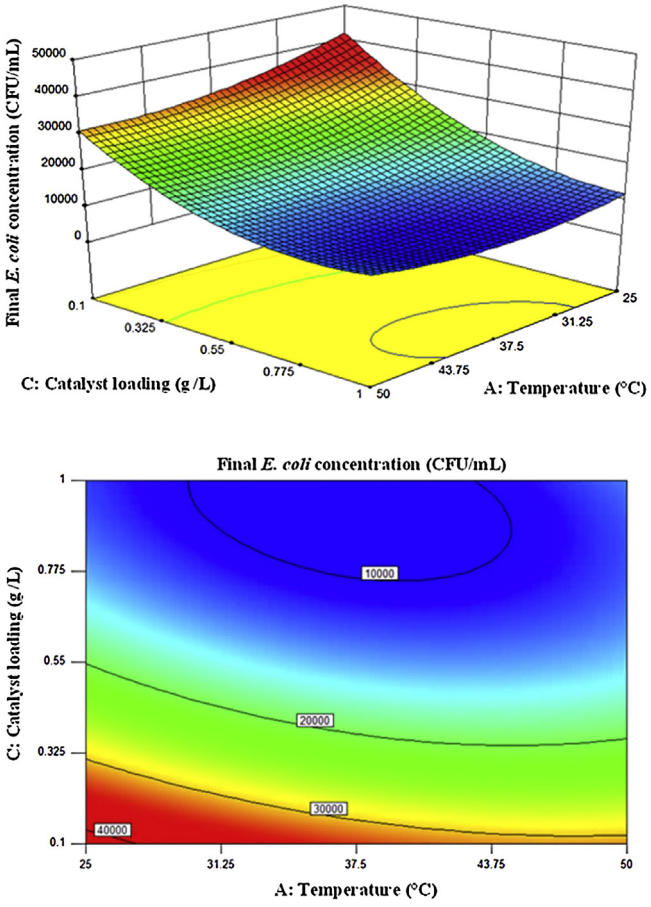

Fig. 4. The response surface plots (a) and contour (b) of the final concentration of *E. coli* as a function of reaction temperature (A) and catalyst loading (C).

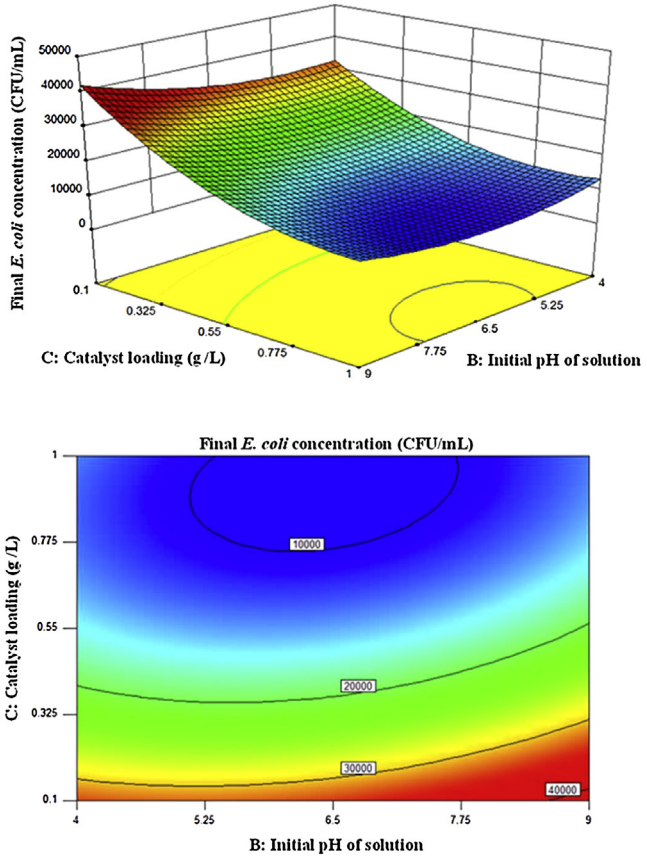

Fig. 5. The response surface plots (a) and contour (b) of the final concentration of *E. coli* as a function of initial pH of solution (B) and catalyst loading (C).

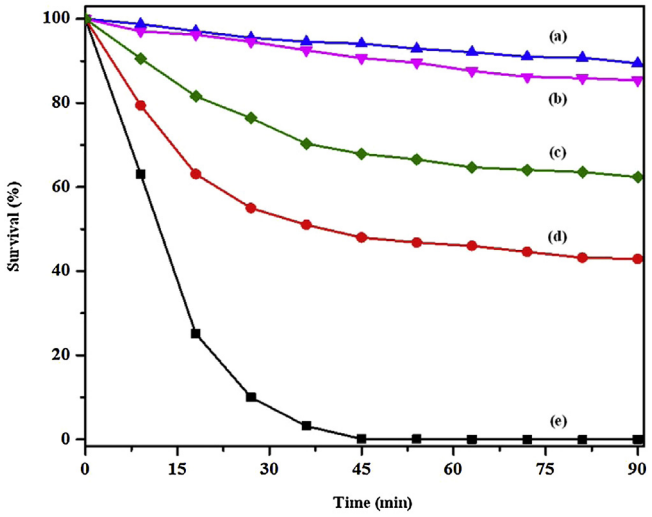

Fig. 6. Time variation of *E. coli* survival (%) under the optimum conditions, using different photocatalysts, with or without light: using Fe–Cd/TiO_2 in the absence of light (a), using visible light in the absence of catalyst (b), using un-promoted TiO_2 under visible light irradiation (c), using TiO_2 P-25 under visible light irradiation (d), and using Fe–Cd/TiO_2 under visible light irradiation (e). At the optimum condition, the initial pH of the solution, reaction temperature and catalyst loading were 40.1 °C, 6.3, and 1.0 g/L, respectively.

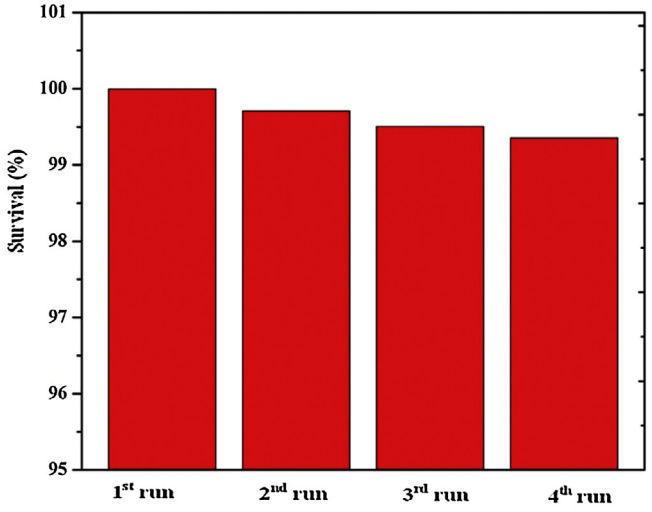

Fig. 7. Reutilization of Fe–Cd/TiO_2 in the inactivation of 10^7 CFU/mL of *E. coli*, under the optimum conditions.

of *E. coli* in these experiments was found to be 10,100 CFU/mL, which is reasonably close to the predicted value. Therefore, the optimum point determined by RSM was successfully verified and suggests that RSM can be a powerful tool for optimizing photocatalytic disinfection processes.

In order to assure that photocatalysis is the dominant mechanism in *E. coli* inactivation, two control experiments were conducted under the optimal conditions; one in the absence of light, and the other in the absence of the Fe–Cd/TiO_2 photocatalyst. As shown in Fig. 6, in both experiments, the disinfection was negligible.

Moreover, use of the synthesized un-promoted TiO_2 clearly shows less activity than Fe–Cd/TiO_2, in agreement with the higher light absorption, and larger surface area of the Fe–Cd/TiO_2 catalyst. It was observed that under optimized conditions and using Fe–Cd/TiO_2, the survived concentration of *E. coli* dropped under 500 CFU/mL in less than 90 min, values required for practical application.

In addition, the photocatalytic performance of TiO_2 P-25 was smaller than un-promoted TiO_2 and co-doped TiO_2 (see Fig. 6). It is somewhat remarkable that the activity of TiO_2 is not zero at wavelengths longer than 400 nm. The main reason is likely the presence of defects in the TiO_2 crystal lattice. The presence of defects in the crystal lattice results in (minor) absorption intensity in the visible light region, in agreement with our optical characterization data (Fig. S5). Several other studies have also shown that bare TiO_2 is slightly photoactive when exposed to visible light [55].

Finally, values of *E. coli* survival (%) in reutilization tests of Fe–Cd/TiO_2 under optimum process conditions are presented in Fig. 7. As can be seen, only minor changes in the performance of the photocatalyst are observed, the conversion-% in all experiments being higher than 99%. Sufficient stability and reusability of the synthesized Fe–Cd/TiO_2 is thus obtained, and leaching of Cd^{2+} or Fe^{3+} ions unlikely, in agreement with the literature [13–18].

4. Conclusions

A novel visible light sensitive photocatalyst, Fe and Cd co-doped TiO_2, was synthesized and applied in water disinfection experiments. For maximizing the antibacterial effect of Fe–Cd/TiO_2 under visible light irradiation, three key operational parameters of a photocatalytic *E. coli* inactivation process were varied using RSM, based on the central composite design of experiments. ANOVA results showed the significance and adequacy of the employed second-order response surface model. Using the obtained response surface and contour plots, the effects of the operational parameters and their interactions on the photocatalytic inactivation of *E. coli* were studied. Based on the proposed model, the optimum values of

initial pH of the solution, reaction temperature and catalyst loading were found to be 40.1 °C, 6.3, and 1.0 g/L, respectively.

Appendix A. Supplementary data

Supplementary data associated with this article can be found, in the online version, at http://dx.doi.org/10.1016/j.apcatb.2014.12.034.

References

[1] A.K. Benabbou, Z. Derriche, C. Felix, P. Lejeune, C. Guillard, Appl. Catal. B 76 (2007) 257–263.
[2] H. Younas, I.A. Qazi, I. Hashmi, M.A. Awan, A. Mahmood, H.A. Qayyum, Environ. Sci. Pollut. Res. 21 (2014) 740–752.
[3] S. Malato, P. Fernandez-Ibanez, M.I. Maldonado, J. Blanco, W. Gernjak, Catal. Today 147 (2009) 1–59.
[4] M.N. Chong, B. Jin, C.W.K. Chow, C. Saint, Water Res. 44 (2010) 2997–3027.
[5] N.M. Al-Bastaki, Chem. Eng. Process. 43 (2004) 935–940.
[6] S. Pigeot-Rémy, F. Simonet, E. Errazuriz-Cerda, J.C. Lazzaronie, D. Atlan, C. Guillard, Appl. Catal. B 104 (2011) 390–398.
[7] S.K. Kansal, A.H. Ali, S. Kapoor, Desalination 259 (2010) 147–155.
[8] J.C. Colmenares, M.A. Aramendia, A. Marinas, J.M. Marinas, F.J. Urbano, Appl. Catal. B 306 (2006) 120–127.
[9] Y.L. Kuo, T.L. Su, F.C. Kung, T.J. Wu, J. Hazard. Mater. 190 (2011) 938–944.
[10] A. Markowska-Szczupaka, K. Ulfigb, A.W. Morawski, Catal. Today 169 (2011) 249–257.
[11] M. Feilizadeh, M. Vossoughi, S.M.E. Zakeri, M. Rahimi, Ind. Eng. Chem. Res. 53 (2014) 9578–9586.
[12] S. Moradi, M. Vossoughi, M. Feilizadeh, S.M.E. Zakeri, M.M. Mohammadi, D. Rashtchian, A.Y. Booshehri, Res. Chem. Intermed. (2014), http://dx.doi.org/10.1007/s11164-013-1519-z.
[13] H.Y. Hao, C.X. He, B.Z. Tian, J.L. Zhang, Res. Chem. Intermed. 35 (2009) 705–715.
[14] K. Obata, K. Kishishita, A. Okemoto, K. Taniya, Y. Ichihashi, S. Nishiyama, Appl. Catal. B 160–161 (2014) 200–203.
[15] H. Yamashita, M. Harada, J. Misaka, M. Takeuchi, B. Neppolian, M. Anpo, Catal. Today 84 (2003) 191–196.
[16] M.R. Mohammadi, D.J. Fray, Acta Mater. 57 (2009) 1049–1059.
[17] C. Karunakaran, A. Vijayabalan, G. Manikandan, P. Gomathisankar, Catal. Commun. 12 (2011) 826–829.
[18] H. Gao, B. Lu, F. Liu, Y. Liu, X. Zhao, Int. J. Photoenergy (2012 (2012) 1–9.
[19] C. Shang, L.M. Cheung, C.M. Ho, M. Zeng, Appl. Catal. B 89 (2009) 536–542.
[20] A.G. Rincon, C. Pulgarin, Appl. Catal. B 44 (2003) 263–284.
[21] P.K.J. Robertson, J.M.C. Robertson, D.W. Bahnemann, J. Hazard. Mater. 211–212 (2012) 161–171.
[22] A.G. Rincon, C. Pulgarin, Appl. Catal. B 51 (2004) 283–302.
[23] S. Sontakke, J. Modak, G. Madras, Appl. Catal. B: Environ. 106 (2011) 453–459.
[24] L. Caballero, K.A. Whitehead, N.S. Allen, J. Verran, J. Photochem. Photobiol. A 202 (2009) 92–98.
[25] A.I. Gomes, J.C. Santos, V.J.P. Vilar, R.A.R. Boaventura, Appl. Catal. B 88 (2009) 283–291.
[26] N. Baram, D. Starosvetsky, J. Starosvetsky, M. Epshtein, R. Armon, Y. Ein-Eli, Appl. Catal. B 101 (2011) 212–219.
[27] D. Gumy, C. Morais, C. Pulgarin, S. Giraldo, R. Hajdu, J. Kiwi, Appl. Catal. B 63 (2006) 76–84.
[28] R.J. Watts, S. Kong, M.P. Orr, G.C. Miller, B.E. Henry, Water Res. 29 (1995) 95–100.
[29] J.A.H. Melian, J.M.D. Rodriguez, A.V. Suarez, E.T. Rendon, C.V.d. Campo, J. Arana, J.P. Pena, Chemosphere 41 (2000) 323–327.
[30] J. Zolgharnein, A. Shahmoradi, J.B. Ghasemi, J. Chemom. 27 (2013) 12–20.
[31] M. Khajeh, M. Gharan, J. Chemom. 28 (2014) 539–547.
[32] M.M. Mohammadia, M. Vossoughi, M. Feilizadeha, D. Rashtchiana, S. Moradia, I. Alemzadeh, Colloids Surf. A: Physicochem. Eng. Aspects 452 (2014) 1–8.
[33] N. Nasralla, M. Yeganeh, Y. Astuti, S. Pitiicharoenphun, N. Shahtahmassebi, A. Kompany, M. Karimipour, B. Mendis, N. Poolton, L. Šiller, Sci. Iran. F 20 (2013) 1018–1022.
[34] J.A. Navio, G. Colh, M.I. Litter, G.N. Bianco, J. Mol. Catal. A 106 (1996) 267–276.
[35] S. Perumal, C.G. Sambandam, K.M. prabu, S. Ananthakumar, Int. J. Res. Eng. Technol. 3 (2014) 651–657.
[36] M. Soleimani, Investigation of The Effect of Semiconductor Nanophotocatalysts on the Bacteria. M. Sc. Thesis, Sharif University of Technology, Tehran, Iran, 2013.
[37] C. Karunakaran, P. Anilkumar, P. Gomathisankar, Chem. Cent. J. 123 (2011) 5–31.
[38] K. Thamaphat, P. Limsuwan, B. Ngotawornchai, J. Nat. Sci. 42 (2008) 357–361.
[39] M. Hamadanian, A. Reisi-Vanani, M. Behpour, A.S. Esmaeily, Desalination 281 (2011) 319–324.
[40] J. Zhu, W. Zheng, B. He, J. Zhang, M. Anpo, J. Mol. Catal. A: Chem. 216 (2004) 35–43.
[41] Y.L. Dong, J.L. Won, S.J. Sung, H.K. Jung, S.K. Yang, Comput. Mater. Sci. 30 (2004) 383.
[42] J. Zhang, D. Fu, Y. Xu, C. Liu, J. Environ. Sci. (China) 22 (8) (2010) 1281–1289.
[43] F. Shahrezaei, Y. Mansouri, A.K. Zinatizadeh, A. Akhbari, Powder Technol. 221 (2012) 203–212.
[44] M. Fathinia, A.R. Khataee, M. Zarei, S. Aber, J. Mol. Catal. A: Chem. 333 (2010) 73–84.
[45] C. Sahoo, A.K. Gupta, J. Hazard. Mater. 215–216 (2012) 302–310.
[46] M. Heyde, R. Portalier, FEMS Microbiol. Lett. 69 (1990) 16–26.
[47] J. Zhou, Y. Zhang, X.S. Zhao, A.K. Ray, Ind. Eng. Chem. Res. 45 (2006) 3503–3511.
[48] W.Y. Wang, Y. Ku, Colloids Surf. Physicochem. Eng. Aspects 302 (2007) 261–268.
[49] A.P. Toor, A. Verma, C.K. Jotshi, P.K. Bajpai, V. Singh, Dyes Pigm. 68 (2006) 53–60.
[50] H. Liao, T. Reitberger, Catalysts 3 (2013) 418–443.
[51] G. Gogniat, M. Thyssen, M. Denis, C. Pulgarin, S. Dukan, FEMS Microbiol. Lett. 258 (2006) 18–24.
[52] U.I. Gaya, A.H. Abdullah, J. Photochem. Photobiol. C 9 (2008) 1–12.
[53] B. Kalmar, L. Greensmith, Adv. Drug Del. Rev. 61 (2009) 310–318.
[54] V.A. Sakkas, P. Calza, C. Medana, A.E. Villioti, Appl. Catal. B 77 (2007) 135–144.
[55] F. Chen, W. Zou, W. Qu, J. Zhang, Catal. Commun. 10 (2009) 1510–1551.